

Constraining SN feedback: a tug of war between reionization and the Milky Way satellites

Jun Hou^{*},¹ Carlos. S. Frenk,¹ Cedric G. Lacey,¹ Sownak Bose¹

¹*Institute for Computational Cosmology, Department of Physics, University of Durham, South Road, Durham, DH1 3LE, UK*

8 December 2024

ABSTRACT

Theoretical models of galaxy formation based on the cold dark matter cosmogony typically require strong feedback from supernova (SN) explosions in order to reproduce the Milky Way satellite galaxy luminosity function and the faint end of the field galaxy luminosity function. However, too strong a SN feedback also leads to the universe reionizing too late, and the metallicities of Milky Way satellites being too low. The combination of these four observations therefore places tight constraints on SN feedback. We investigate these constraints using the semi-analytical galaxy formation model GALFORM. We find that these observations favour a SN feedback model in which the feedback strength evolves with redshift. We also investigate the sources of the photons responsible for reionization, and find that, for our best fit model, half of the ionizing photons are emitted by galaxies with rest-frame far-UV absolute magnitudes $M_{\text{AB}}(1500\text{\AA}) < -17.5$, which implies that already observed galaxy populations contribute about half of the photons responsible for reionization. The $z = 0$ descendants of these galaxies are mainly galaxies with stellar mass $M_* > 10^{10} M_\odot$ and preferentially inhabit halos with mass $M_{\text{halo}} > 10^{13} M_\odot$.

Key words: galaxies: evolution – galaxies: formation – galaxies: high-redshift

1 INTRODUCTION

Supernova feedback (SN feedback hereafter) is a very important physical process for regulating the star formation in galaxies (Larson 1974; Dekel & Silk 1986; White & Frenk 1991). Despite its importance, SN feedback is not well understood. Perhaps the best way to improve our understanding of this process is by investigating its physical properties using hydrodynamical simulations. This, however, is very difficult to achieve with current computational power: cosmological hydrodynamical simulations (e.g. Davé et al. 2013; Vogelsberger et al. 2014; Schaye et al. 2015) can provide large galaxy samples and can follow galaxy evolution spanning the history of the Universe, but do not have high enough resolution to follow individual star forming regions, which is needed to understand the details of SN feedback; conversely high resolution hydrodynamical simulations (e.g. Bate 2012; Hopkins et al. 2012) can resolve many more details of individual star forming regions, but do not provide a large sample and cannot follow a long period of evolution. Because of these limitations, it is worth trying to improve our understanding of SN feedback in alternative ways. One promising approach is to extract constraints on SN feedback from the-

oretical models of galaxy formation combined with observational constraints.

Among all relevant observations, a combination of four observables may be particularly effective because they constrain the strength of feedback in opposite directions. These are the abundance of faint galaxies, including both the faint ends of the $z = 0$ field galaxy luminosity function (hereafter field LF) and the Milky Way satellite luminosity function (hereafter MW sat LF), the Milky Way satellite stellar metallicity vs. stellar mass correlation (hereafter MW sat $Z_* - M_*$ correlation) and the redshift, $z_{\text{re, half}}$, at which the Universe was 50% reionized. The observed abundance of faint galaxies is very low compared to the abundance of low mass dark matter halos in the standard cold dark matter (CDM) model of cosmogony (e.g. Benson et al. 2003; Moore et al. 1999; Klypin et al. 1999), which cannot be reproduced by very weak SN feedback, and this puts a lower limit on the SN feedback strength. On the other hand, $z_{\text{re, half}}$ and the MW sat $Z_* - M_*$ correlation put upper limits on the SN feedback strength, because too strong a SN feedback would cause too strong a metal loss and a suppression of star formation in galaxies, thus leading to too low Z_* at a given M_* , and too low $z_{\text{re, half}}$. Also note that this combination of observations constrains SN feedback over a wide range of galaxy types and redshifts: the field LF mainly provides constraints on SN feedback in larger galaxies, with circular

* E-mail: jun.hou@durham.ac.uk

velocity $V_c \gtrsim 80 \text{ km s}^{-1}$, while $z_{\text{re, half}}$ mainly constrains SN feedback at $z \gtrsim 8$, and the Milky Way satellite observations (MW sat LF and MW sat $Z_* - M_*$ correlation) provide constraints on the SN feedback in very small galaxies, i.e. $V_c \lesssim 40 \text{ km s}^{-1}$, and probably over a wide redshift range, from very high redshift to $z \sim 1$. (This is because recent observations (e.g. de Boer et al. 2012; Vargas et al. 2013) indicate that the Milky Way satellites have diverse star formation histories, with some of them forming all of their stars very early, and others having very extended star formation histories.)

In this work, we investigate the constraints placed by this combination of observations on SN feedback using the semi-analytical galaxy formation model GALFORM (Cole et al. 2000; Baugh et al. 2005; Bower et al. 2006; Lacey et al. 2015). A semi-analytical galaxy formation model is ideal for this aim, because with it one can generate large samples of galaxies with high mass resolution, which is important for simulating both Milky Way satellites and star formation at high redshift, and it is also computationally feasible to explore various physical models and parameterizations.

This paper is organized as follows. Section 2 describes the starting point of this work, the Lacey et al. (2015) (hereafter Lacey15) GALFORM model, as well as extensions of this model and details of the simulation runs. Section 3 presents the results from the Lacey15 and modified models. Section 4 discusses the physical motivation for some of the modifications, and also which galaxies drive cosmic reionization and what their $z = 0$ descendants are. Finally a summary and conclusions are given in Section 5.

2 METHODS

2.1 Starting point: Lacey15 model

The basic model used in this work is the Lacey15 (Lacey et al. 2015) model, a recent version of GALFORM. This model, and the variants of it that we consider in this paper, all assume a flat Λ CDM universe with cosmological parameters based on the WMAP-7 data (Komatsu et al. 2011): $\Omega_{\text{m}0} = 0.272$, $\Omega_{\text{v}0} = 0.728$, $\Omega_{\text{b}0} = 0.0455$ and $H_0 = 70.4 \text{ km s}^{-1} \text{ Mpc}^{-1}$, and an initial power spectrum with slope $n_s = 0.967$ and normalization $\sigma_8 = 0.810$. The Lacey15 model implements sophisticated modeling of disk star formation, improved treatments of dynamical friction on satellite galaxies and of starbursts triggered by disk instabilities and an improved stellar population synthesis model; it reproduces a wide range of observations, including field galaxy luminosity functions from $z = 0$ to $z = 3$, galaxy morphological types at $z = 0$, and the number counts and redshift distribution of submillimetre galaxies. An important feature of this model is that it assumes a top-heavy IMF for stars formed in starbursts, which is required to fit the submillimetre data, while stars formed by quiescent star formation in disks have a Solar neighbourhood IMF. Stellar luminosities of galaxies at different wavelengths, and the production of heavy elements by supernovae, are predicted self-consistently, allowing for the varying IMF.

SN feedback is modeled in this and earlier versions of GALFORM as follows. SN feedback ejects gas out of galaxies, and thus reduces the amount of cold gas in galaxies, regulat-

ing the star formation. The gas ejection rate is formulated as:

$$\dot{M}_{\text{eject}} = \beta\psi, \quad (1)$$

where \dot{M}_{eject} is the mass ejection rate, ψ is the star formation rate and the mass-loading factor, β , encodes the details of SN feedback models. In the approximation of instantaneous recycling that we use here, in which we neglect the time delay between the birth and death of a star, the supernova rate, and hence also the supernova energy injection rate, are proportional to the instantaneous star formation rate ψ .

In the Lacey15 model, β is set to be a single power law in galaxy circular velocity, V_c , specifically,

$$\beta = \left(\frac{V_c}{V_{\text{SN}}} \right)^{-\gamma_{\text{SN}}}, \quad (2)$$

where V_{SN} and γ_{SN} are two free parameters. In the Lacey15 model, $V_{\text{SN}} = 320 \text{ km s}^{-1}$ and $\gamma_{\text{SN}} = 3.2$. β as a function of V_c for the Lacey15 model is illustrated in the left panel of Fig. 1.

As shown in Figs. 3 and 5, the above single power-law SN feedback model is disfavored by the combination of the four observational constraints mentioned in §1. We therefore investigate some modified SN feedback models and test them against the same set of observations. These modified models are described next.

2.2 Modified SN feedback models

In the modified SN feedback models we assume a broken power law for β , with a change in slope below a circular velocity, V_{thresh} :

$$\beta = \begin{cases} (V_c/V_{\text{SN}})^{-\gamma_{\text{SN}}} & V_c \geq V_{\text{thresh}} \\ (V_c/V'_{\text{SN}})^{-\gamma'_{\text{SN}}} & V_c < V_{\text{thresh}} \end{cases}. \quad (3)$$

Here V_{SN} , γ_{SN} , V_{thresh} and γ'_{SN} are free parameters, while V'_{SN} is fixed by the condition that the two power laws should join at $V_c = V_{\text{thresh}}$.

2.2.1 Saturated feedback model

In this class of models we set $\gamma'_{\text{SN}} < \gamma_{\text{SN}}$, so that the mass-loading factor, β , for $V_c < V_{\text{thresh}}$ is lower than in the single power-law model. Note that we require $\gamma'_{\text{SN}} \geq 0$, because a negative γ'_{SN} would predict an anti-correlation between galaxy stellar metallicity and stellar mass, in contradiction with observations of the MW satellites.

A similar feedback model, with $\gamma'_{\text{SN}} = 0$, was previously used by Font et al. (2011), which showed that it improved the agreement of GALFORM model predictions with Milky Way observations. However, in the present work, the observational constraints are more stringent than in Font et al. (2011), because here not only are Milky Way observations considered, but also the field LF and the reionization redshift.

In this work, we investigate a specific saturated feedback model, with $V_{\text{thresh}} = 75 \text{ km s}^{-1}$ and $\gamma'_{\text{SN}} = 0$, which implies that β is a constant for galaxies with $V_c < 75 \text{ km s}^{-1}$, and is the same as that given by the Lacey15 model when $V_c > V_{\text{thresh}}$. We call this specific saturated feedback model SatFb. The mass-loading factor for this model is also illustrated in the left panel of Fig. 1.

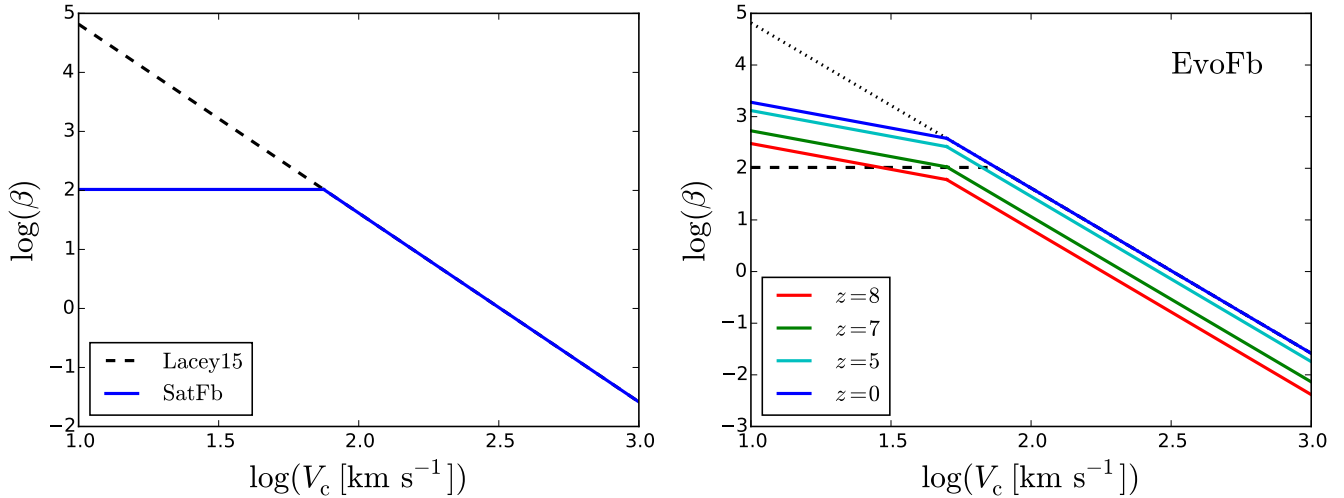


Figure 1. Illustration of the different supernova feedback models used in this work. **Left panel:** The dashed black line shows the mass-loading factor, β , as a function of circular velocity, V_c , in the Lacey15 model, while the solid blue line shows β for the SatFb model. **Right panel:** β for the EvoFb model. Different colours indicate different redshifts. β for the Lacey15 and SatFb models are also plotted for reference, and are shown by the black dotted and dashed lines respectively.

2.2.2 Evolving feedback model

This model has weaker SN feedback strength at higher redshift. Here we investigate a specific model, which has $\gamma_{\text{SN}} = 3.2$ (as in Lacey15), $\gamma'_{\text{SN}} = 1.0$, $V_{\text{thresh}} = 50 \text{ km s}^{-1}$ and

$$V_{\text{SN}} [\text{km s}^{-1}] = \begin{cases} 180 & z > 8 \\ -35z + 460 & 4 \leq z \leq 8 \\ 320 & z < 4 \end{cases} . \quad (4)$$

For $V_c > 50 \text{ km s}^{-1}$, this model has the same SN feedback strength as the Lacey15 model at $z < 4$, but weaker feedback strength at $z > 4$. There is also a saturation of the SN feedback strength in small galaxies with $V_c < 50 \text{ km s}^{-1}$; however, the modification is weaker than that in the SatFb model. The general behaviour of this model is motivated by the results of Lagos et al. (2013), who predicted mass-loading factors from a detailed model of SN-driven superbubbles expanding in the ISM. (The Lagos et al. model was however incomplete, in that it considered only mass ejection out of the galaxy disk, but not out of the halo.) The mass loading factor, β , for this model is illustrated in the right panel of Fig. 1. We call this model EvoFb.

The physical motivation for introducing the redshift evolution in the SN feedback will be discussed further in §4.

2.3 The redshift of reionization and photoionization feedback

We estimate the redshift of reionization predicted by a GALFORM model by calculating the ratio, $\mathcal{R}(z)$, of the number density of ionizing photons produced up to that redshift to the number density of hydrogen nuclei:

$$\mathcal{R}(z) = \frac{\int_z^\infty \epsilon(z') dz'}{n_{\text{H}}} , \quad (5)$$

where $\epsilon(z')$ is the number of hydrogen-ionizing photons produced per unit comoving volume per unit redshift at redshift

z' , and n_{H} is the comoving number density of hydrogen nuclei.

The Universe is assumed to be fully ionized at a redshift, $z_{\text{re,full}}$, for which,

$$\mathcal{R}(z_{\text{re,full}}) = \frac{1 + N_{\text{rec}}}{f_{\text{esc}}} , \quad (6)$$

where N_{rec} is the mean number of recombinations per hydrogen atom up to reionization, and f_{esc} is the fraction of ionizing photons that can escape from the galaxies producing them into the IGM. Following Raičević et al. (2011), we adopt $N_{\text{rec}} = 1$ and $f_{\text{esc}} = 0.2$, and thus the threshold for reionization is $\mathcal{R}(z_{\text{re,full}}) = 10$.

Observations of the CMB directly constrain the electron scattering optical depth to recombination, which is then converted to a reionization redshift by assuming a simple model for the redshift dependence of the ionized fraction. Papers by the *WMAP* and *Planck* collaborations (e.g. Planck Collaboration et al. 2014) typically express the reionization epoch in terms of the redshift, $z_{\text{re,half}}$, at which the IGM is 50% ionized, by using the simple model for non-instantaneous reionization described in Appendix B of Lewis (2008). For comparing with such observational estimates, we therefore calculate $z_{\text{re,half}}$ from GALFORM by assuming $\mathcal{R}(z_{\text{re,half}}) = \frac{1}{2} \mathcal{R}(z_{\text{re,full}})$. For the above mentioned choices of N_{rec} and f_{esc} , this is equivalent to $\mathcal{R}(z_{\text{re,half}}) = 5$.

Reionization may suppress galaxy formation in small halos, an effect called photoionization feedback (Couchman & Rees 1986; Efstathiou 1992; Thoul & Weinberg 1996). In this work, the photoionization feedback is modeled using a simple approximation (Benson et al. 2003), in which dark matter halos with circular velocity at the virial radius $V_{\text{vir}} < V_{\text{crit}}$ have no gas accretion or gas cooling for $z < z_{\text{crit}}$. As shown by Benson et al. (2002) and Font et al. (2011), this method provides a good approximation to a more complex, self-consistent photoionization feedback model. Here, V_{crit} and z_{crit} are two free parameters. In this paper, unless otherwise specified, we adopt $z_{\text{crit}} = z_{\text{re,full}}$ and $V_{\text{crit}} = 30 \text{ km s}^{-1}$.

This value of V_{crit} is consistent with the hydrodynamical simulation results of Okamoto et al. (2008). Note that this method does not necessarily imply that star formation in galaxies in halos with $V_{\text{vir}} < V_{\text{crit}}$ is turned off immediately after $z = z_{\text{re,full}}$. The star formation in these galaxies can continue as long as the galaxy cold gas reservoir is not empty.

2.4 Simulation runs

Studying reionization requires resolving galaxy formation in low mass halos ($M_{\text{vir}} \sim 10^8 - 10^{10} M_{\odot}$) at high redshifts ($z \sim 7 - 15$), and thus very high mass resolution for the dark matter halo merger trees. The easiest way to achieve this high resolution is to use Monte Carlo (MC) merger trees.

Studying the properties of the Milky Way satellites also requires very high mass resolution because the host halos of these small satellites are small. This too is easily achieved using MC merger trees. Furthermore, because building MC merger trees is computationally inexpensive, it is possible to build a large statistical sample of Milky Way-like halos to study their satellites.

In this work we generate MC merger trees using the method of Parkinson et al. (2008). To study reionization, we ran simulations starting at $z_{\text{start}} = 20$ down to different final redshifts, z_{end} , to derive $\epsilon(z)$ defined in Eq (5) at $z = 5 - 15$ and the $z = 0$ field LF. We scale the minimum progenitor mass in the merger trees as $(1 + z_{\text{end}})^{-3}$, with a minimum resolved mass, $M_{\text{res}} = 7 \times 10^9 M_{\odot}$ for $z_{\text{end}} = 0$. We have tested that these choices are sufficient to derive converged results. For the Milky Way satellite study, the present-day host halo mass is chosen to be in the range $5 \times 10^{11} - 2 \times 10^{12} M_{\odot}$, which represents the current observational constraints on the halo mass of the Milky Way, and we sample this range with five halo masses evenly spaced in $\log(\text{mass})$. For each of these halo masses, GALFORM is run on 100 MC merger trees, with minimum progenitor mass $M_{\text{res}} = 1.4 \times 10^6 M_{\odot}$, which is small enough for modeling the Milky Way satellites, and $z_{\text{start}} = 20$ and $z_{\text{end}} = 0$. We do not attempt to select Milky Way-like host galaxies, because we found that the satellite properties correlate better with the host halo mass than with the host galaxy properties.

3 RESULTS

In this section, we show how the results from the different models compare with the key observational constraints that we have identified, namely: the field galaxy luminosity functions at $z = 0$; the redshift of reionization; the MW satellite galaxy luminosity function; and the stellar metallicity vs stellar mass relation for MW satellites.

3.1 Lacey15 model

We begin by showing the results for the default Lacey15 model, since this then motivates considering models with modified SN feedback. Fig. 2 shows the b_J - and K -band field LFs of different models at $z = 0$ (left and right panels respectively). The dashed blue lines show the LFs calculated using N-body merger trees, as used in the original Lacey et al. (2015) paper to calibrate the model parameters. The fit to the observed LFs is seen to be very good. The solid blue

lines show the predictions with identical model parameters but instead using MC merger trees, as used in the remainder of this paper. The run with MC merger trees gives slightly lower LFs than the run with the N-body trees around the knee of the LF, but at lower luminosities, the results predicted using MC and N-body merger trees are in good agreement. We remind the reader that we use MC merger trees in the main part of this paper in order to achieve the higher halo mass resolution that we need for the other observational comparisons. Since the differences in the LFs between the two types of merger tree are small, and barely affect the faint end of the field LFs which are the main focus of interest here, we do not consider them important for this paper.

Fig. 3 shows the predicted $\mathcal{R}(z)$ (defined in Eq 5) for different SN feedback models. In each panel, the horizontal black dashed line indicates the criterion for 50% reionization, i.e. $\mathcal{R}(z_{\text{re, half}}) = 5$, the vertical black dashed line indicates $z_{\text{re, half}}$ of the corresponding model, and the corresponding value of $z_{\text{re, half}}$ is given in the panel. The gray shaded area in each of these panels indicates the current observational constraint from *Planck*, namely $z_{\text{re}} = 8.8_{-1.4}^{+1.7}$ (68% confidence region, Planck Collaboration et al. 2015). The redshift $z_{\text{re, full}}$ for full reionization (given by $\mathcal{R}(z_{\text{re, full}}) = 10$) for each model is also given in the corresponding panel. The results for the Lacey15 model are shown in the left panel. With the above mentioned criterion, this model predicts $z_{\text{re, half}} = 6.1$, which is too low compared to the observational estimate. This indicates that in the Lacey15 model, star formation at high redshift, $z \gtrsim 8$, is suppressed too much. There are two possible reasons for this oversuppression: one is the SN feedback at high redshift is too strong, and the other is that the SN feedback in low-mass galaxies is too strong (since the typical galaxy mass is lower at higher redshift).

Fig. 4 shows the cumulative luminosity function of satellite galaxies in Milky Way-like host halos. In each panel, the red solid and dashed lines show the simulation results for the corresponding model. For each model, the simulations were run on 100 separate merger trees for each of 5 host halo masses, evenly spaced in the logarithm of the mass in the range $5 \times 10^{11} - 2 \times 10^{12} M_{\odot}$. This simulated sample of MW-like halos contains 500 halos in total, and the red solid line shows the median satellite LF for this sample, while the red dashed lines indicate the 5–95% range. The black solid line in each panel shows the observed Milky Way satellite luminosity function. For $M_V < -11$, we plot the direct observational measurement from McConnachie (2012). For these brighter magnitudes, current surveys for MW satellites are thought to be complete over the whole sky. For $M_V \geq -11$ we plot the observational estimate from Kopev et al. (2008) based on SDSS, which includes corrections for incompleteness due to both partial sky coverage and in detecting satellites in imaging data. The predictions for the Lacey15 model are shown in the upper left panel, and are in very good agreement with the observations.

Fig. 5 shows the $Z_* - M_*$ correlation for satellite galaxies in Milky Way-like host halos. The sample is the same as that for Fig. 4. In each panel, the red solid line shows the median of the sample, while the red dashed lines indicate the 5–95% range. The black filled circles in each panel show observational data. We have converted the observed $[\text{Fe}/\text{H}]$ values into the total stellar metallicities, Z_*/Z_{\odot} , by assuming that the chemical abundance patterns in the ob-

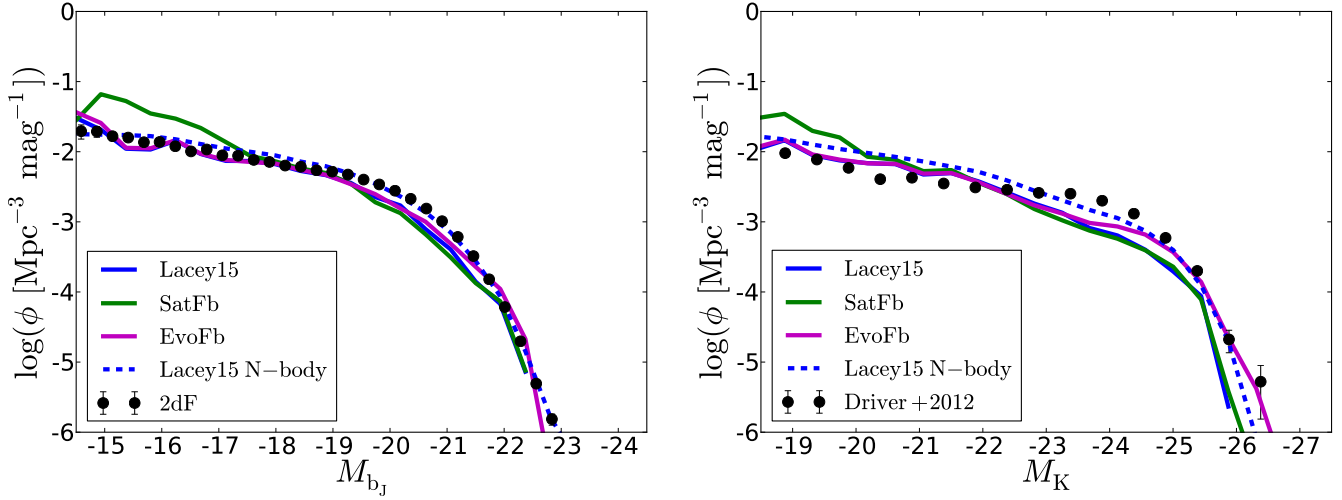


Figure 2. $z = 0$ field luminosity functions. The left panel shows the b_J -band luminosity function and the right panel the K -band luminosity function. In both panels, the different colour solid lines show the predictions using Monte Carlo merger trees for different SN feedback models, as indicated in the line key, while the blue dashed lines are for the Lacey15 model run with N-body merger trees. The black points with errorbars are observational data, from Norberg et al. (2002) for the b_J -band and from Driver et al. (2012) for the K -band.

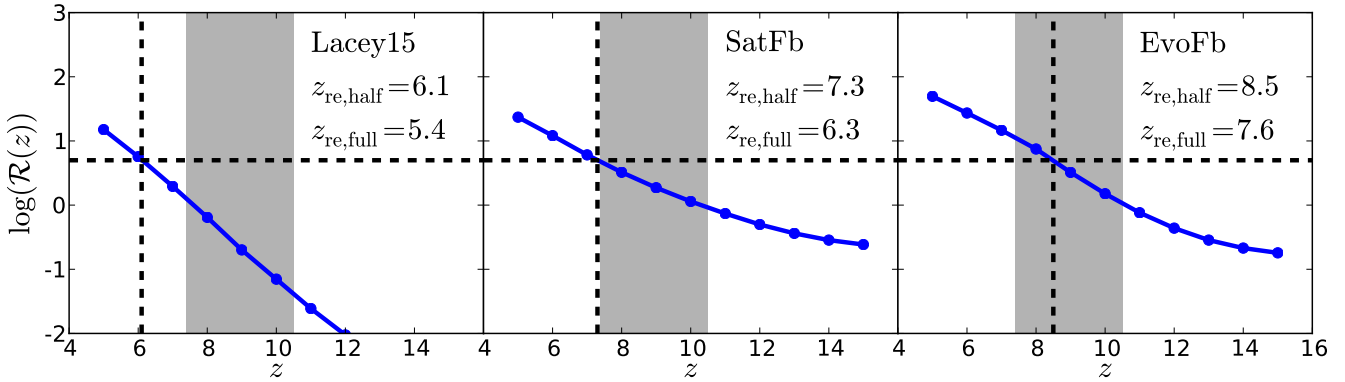


Figure 3. $\mathcal{R}(z)$, which is the ratio of the total number of ionizing photons produced up to redshift z to the total number of hydrogen nuclei, for different SN feedback models. Each panel shows a different model, as labelled. The blue line shows the predicted $\mathcal{R}(z)$, while the horizontal dashed line shows the threshold $\mathcal{R}(z_{\text{re, half}}) = 5$ for 50% reionization, and the vertical dashed line the corresponding redshift $z_{\text{re, half}}$. The grey shaded region shows the observational constraint on $z_{\text{re, half}}$ from *Planck*, namely $z_{\text{re}} = 8.8_{-1.4}^{+1.7}$ (68% confidence region, Planck Collaboration et al. 2015). The predicted value of the redshift $z_{\text{re, full}}$ for 100% reionization is also given in each panel.

served satellites are the same as in the Sun. This assumption may lead to an underestimation of the metallicities of low mass satellites, which may not have had enough enrichment by Type Ia supernova to reach the Solar pattern. For these satellites, the observed Z_* values shown in the figure are therefore effectively lower limits. The results of the Lacey15 model are again shown in the upper left panel. The $Z_* - M_*$ relation predicted by this model is about an order of magnitude below the observations. Because the discrepancy in metallicity is about one order of magnitude, it cannot be caused by inaccuracies in the theoretical stellar yields of metals in this model. These yields are obtained by integrating the yields predicted by stellar evolution models over the IMFs assumed for stars formed either quiescently or in starbursts. Assuming that the true metal yields are similar to what is assumed in the model, then for a given stellar mass, the total metals produced are fixed, so the low metallicities

seen in the Lacey15 model imply that the loss of metals from satellite galaxies is excessive. Since the metal loss is caused by the outflows induced by SN feedback, this indicates that the SN feedback in these small galaxies is too strong.

In summary, the Lacey15 model motivates two types of modification to the SN feedback. One is suppressing SN feedback in small galaxies, which is the saturated feedback model. The other one is suppressing SN feedback at high redshift, i.e. $z \geq 8$, but keeping strong feedback at $z < 4$ in order to reproduce the $z = 0$ field LFs. This corresponds to the evolving feedback model. Below, these two kinds of modification will be tested one at a time.

3.2 Saturated feedback model (SatFb)

The solid green lines in Fig. 2 show the b_J -band and K -band LFs for the SatFb model. It is clear that by reducing

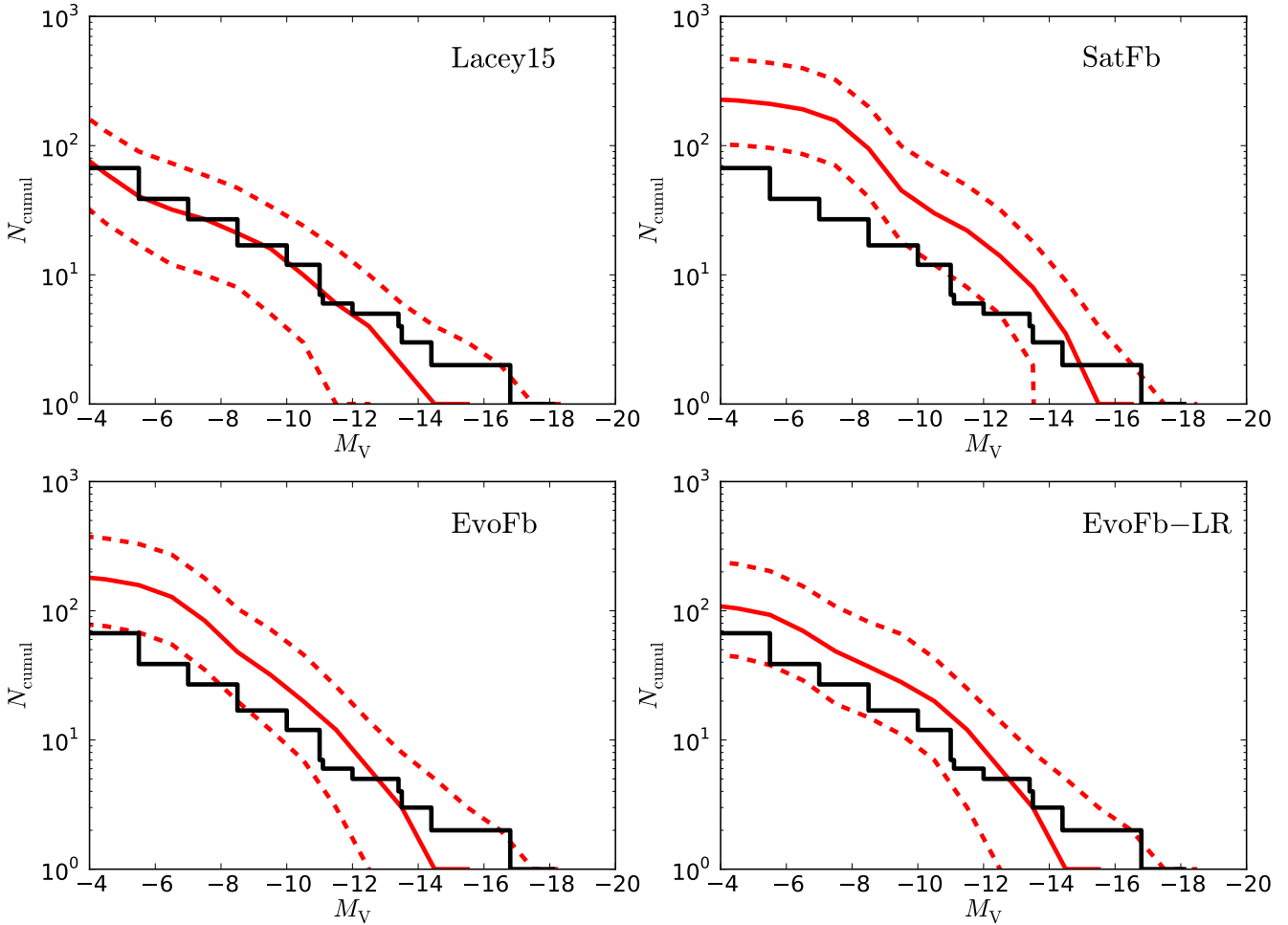


Figure 4. Cumulative luminosity function of satellite galaxies in Milky Way-like host halos at $z = 0$. In each panel, the red lines show the model predictions, with the red solid line showing the median for a sample of MW-like halos, and the red dashed lines indicating the 5–95% range. The black solid line in each panel is the observed Milky Way satellite cumulative luminosity function. For $M_V < -11$, the black solid line shows the direct observational results from McConnachie (2012), while for $M_V \geq -11$, it shows the results from Koposov et al. (2008), who applies some corrections for incompleteness in the observations.

the SN feedback strength in galaxies with $V_c < 75 \text{ km s}^{-1}$, the predicted faint ends of both field LFs become steeper, and in poorer agreement with observations. Although the discrepancy is only about a factor of 2, it can be observed in a relatively wide magnitude range. The field LF comparison thus suggests that the SN feedback is suppressed too much in this model.

The middle panel of Fig. 3 shows $\mathcal{R}(z)$ for the SatFb model, and the corresponding $z_{\text{re,half}}$ is 7.3. This $z_{\text{re,half}}$ is just outside the $1\text{-}\sigma$ region of the *Planck* observations, and so is marginally consistent with these data. From the point of view of predicting early enough reionization, the SN feedback strength in the current SatFb model is therefore an upper limit.

The upper right panel of Fig. 4 shows the satellite luminosity function of the Milky Way-like host halos in the SatFb model. Because the SN feedback is suppressed in small galaxies, the faint end of the luminosity function is now too high, with too many faint ($M_V \geq -8$) satellites. But note that these faint Milky Way satellites are very small galaxies, and thus the excess in the faint end of the MW

sat LF might be reduced by adjusting the photoionization feedback. However, this would not help to reduce the excess at the faint ends of the field LFs, because the galaxies there are larger and not very sensitive to photoionization feedback. The upper right panel of Fig. 5 shows the satellite $Z_* - M_*$ correlation for the Milky Way-like host halos. This correlation is very shallow, because most of these satellites have $V_c < V_{\text{thresh}} = 75 \text{ km s}^{-1}$, so they all have similar β . The SatFb model predicts metallicities of satellites with $M_* \leq 10^4 M_\odot$ that are higher than the observations by a factor of a few. Together, these results from the Milky Way-like host halos suggest that the SN feedback in small galaxies is suppressed too much.

This SatFb model therefore does not provide a solution to the problems identified in the Lacey15 model. Further adjustments within the framework of the saturated feedback model would involve changing the saturated power-law slope γ'_{SN} and/or the threshold velocity, V_{thresh} . In the present SatFb model, as mentioned above, γ'_{SN} is already at its lower limit, namely 0, and introducing a positive γ'_{SN} only leads to a stronger SN feedback in small galaxies than

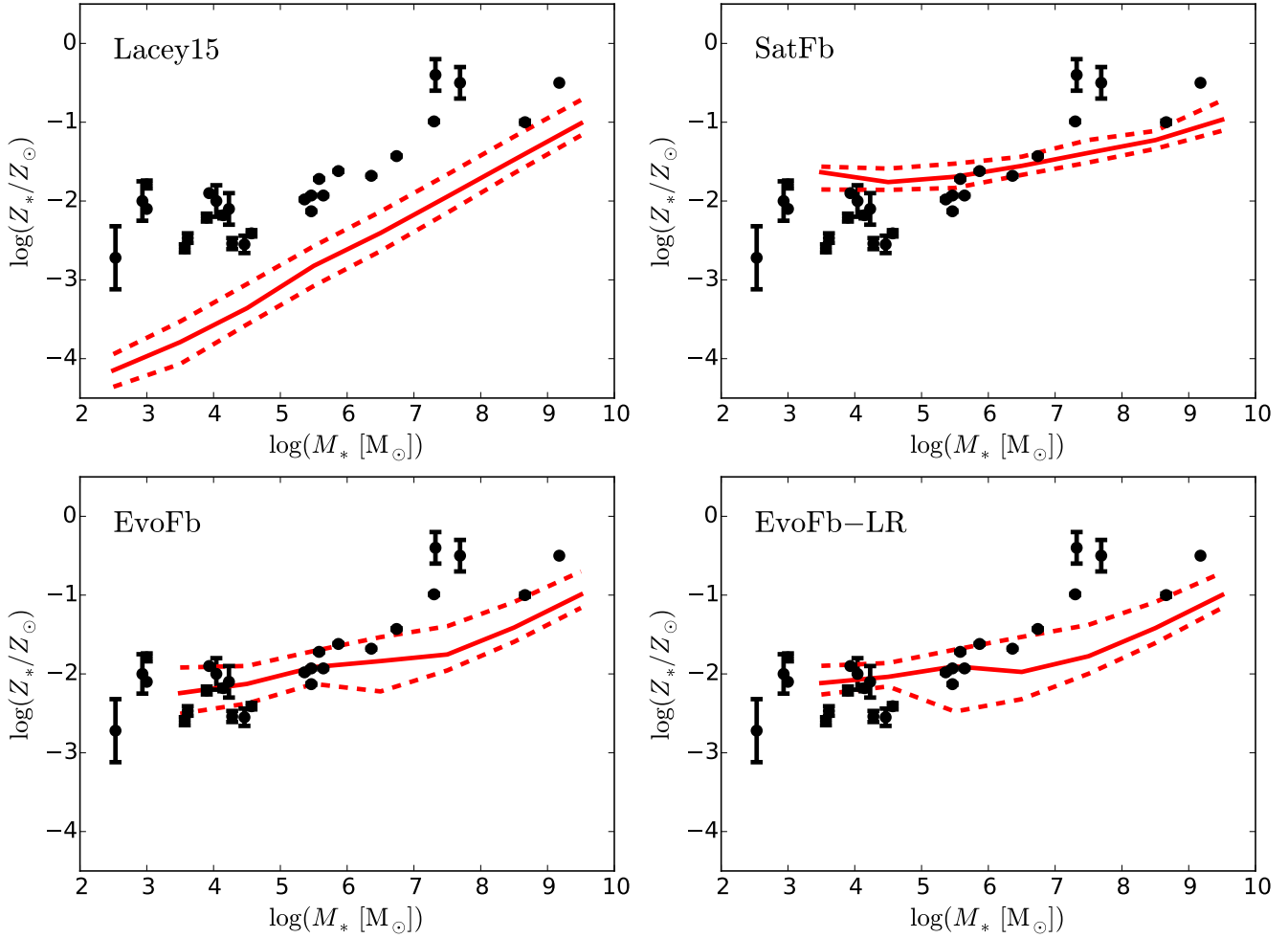


Figure 5. The stellar metallicity (Z_*) vs stellar mass (M_*) relation for satellite galaxies in Milky Way-like host halos at $z = 0$. The simulated sample for each model is the same as in Fig. 4. In each panel, the red solid line shows the median of the simulated sample, while the red dashed lines indicate the 5 – 95% range. The black filled circles show the observational results compiled by McConnachie (2012). The observed $[\text{Fe}/\text{H}]$ values in McConnachie (2012) are converted into the total stellar metallicities, Z_*/Z_\odot , in Solar units by assuming the chemical patterns of the observed satellites are Solar. The total metallicities, Z_* , predicted by the model, which are absolute values, are converted into Solar units assuming $Z_\odot = 0.0142$ (Asplund et al. 2009).

in the current SatFb model, and this would not predict a high enough $z_{\text{re, half}}$. Reducing V_{thresh} would also lead to a stronger SN feedback in small galaxies than in the current SatFb model, so would not improve the prediction for $z_{\text{re, half}}$ either, while enhancing V_{thresh} would lead to a saturation of the SN feedback in even larger galaxies and a stronger saturation in small galaxies than in the current SatFb model, thus further spoiling the field LFs, MW sat LF and MW sat $Z_* - M_*$ correlation. The saturated feedback model therefore seems disfavored by this combination of observational constraints.

3.3 Evolving feedback model (EvoFb)

The magenta lines in Fig. 2 show the b_J-band and K-band field LFs in the EvoFb model. The results are almost identical to those in the Lacey15 model, and the faint ends are well reproduced. This is because in the EvoFb model, the

SN feedback in galaxies with $V_c \geq 50 \text{ km s}^{-1}$ at $z \leq 4$ is the same as in the Lacey15 model.

The right panel in Fig. 3 shows $\mathcal{R}(z)$ for the EvoFb model; the corresponding $z_{\text{re, half}}$ is 8.5, which is in agreement with the observations. Since the EvoFb model adopts a saturation in the feedback which is weaker than that in the SatFb model, but nonetheless predicts a higher $z_{\text{re, half}}$, the improvement in $z_{\text{re, half}}$ must be mainly caused by the introduction of the redshift evolution of the SN feedback.

The lower left panel of Fig. 4 shows the satellite luminosity function of the Milky Way-like host halos in the EvoFb model. The model predictions are roughly consistent with the observations, although the very faint end ($M_V \geq -8$) of the MW sat LF is somewhat too high (but better than in the SatFb model). However, the observations of this very faint end have significant uncertainties, so this model is still acceptable. The lower left panel of Fig. 5 shows the $Z_* - M_*$ relation for the satellite galaxies in Milky Way-like host halos in the EvoFb model. The model predictions are now roughly consistent with the observations. This im-

provement is achieved by adopting both an evolving SN feedback and a saturation of the SN feedback strength in galaxies with $V_c \leq 50 \text{ km s}^{-1}$.

Because the predictions for Milky Way satellites are sensitive to the photoionization feedback, it is possible to further improve the agreement with observations for these galaxies by adjusting the photoionization feedback. One possible adjustment is to adopt the so-called local reionization model (see Font et al. (2011) and references therein), in which higher density regions reionize earlier, so that $z_{\text{re,full}}$ for the Local Group region is earlier than the global average $z_{\text{re,full}}$ constrained by the *Planck* data. Earlier reionization means earlier photoionization feedback, so that for the Milky Way satellites one has $z_{\text{crit}} > z_{\text{re,full}}$. Font et al. (2011) adopted a detailed model to study this local reionization effect, and suggested that using $z_{\text{crit}} = 10$ gives a good approximation to the results of the more detailed model. Here we also adopt $z_{\text{crit}} = 10$, and we label the model with evolving SN feedback and $z_{\text{crit}} = 10$ as EvoFb-LR.

We tested that the predictions for global properties like $z_{\text{re,full}}$, $z_{\text{re,half}}$ and the field LFs are not very sensitive to the value of z_{crit} . It is therefore justified to ignore the variation of z_{crit} with local density when calculating these global properties, and adopt a single $z_{\text{crit}} = z_{\text{re,full}}$ when predicting these. This also means that introducing such a local reionization model does not allow one to bring the standard Lacey15 or SatFb models into agreement with all of our observational constraints, since some of the discrepancies described above involve these global properties.

The lower right panel of Fig. 4 shows the satellite luminosity function of the Milky Way-like host halos in the EvoFb-LR model. The model predictions agree with observations better than the EvoFb model, because the abundance of the very faint satellites is reduced by the enhanced photoionization feedback. The lower right panel of Fig. 5 shows the $Z_* - M_*$ relation for satellite galaxies in Milky Way-like host halos for the EvoFb-LR model. The rough agreement with observations previously found for the EvoFb model is seen to be preserved in the EvoFb-LR variant.

4 DISCUSSION

4.1 Why should the SN feedback strength evolve with redshift?

The physical idea behind formulating the mass loading factor, β , of SN-driven outflows (Eq 1) as a function of V_c is that the strength of the SN feedback driven outflows (for a given star formation rate, ψ) depends on the gravitational potential well, and V_c is a proxy for the depth of the gravitational potential well. However, in reality the strength of outflows does not only depend on the gravitational potential well, but may also depend on the galaxy gas density, gas metallicity and molecular gas fraction. This is because the gas density and metallicity determine the local gas cooling rate in the ISM, which determines the fraction of the injected SN energy that can finally be used to launch outflows, while the dense molecular gas in galaxies may not be affected by the SN explosions, and thus may not be ejected as outflows. These additional factors may evolve with redshift, and V_c may not be a good proxy for them, so if the outflow mass

loading factor, β , is still formulated as a function of V_c only, a single function may not be valid for all redshifts and some redshift evolution of β may need to be introduced.

The detailed dependence of β on the galaxy gas density, gas metallicity and molecular gas fraction can only be derived by using a model which considers the details of the ISM. The model of Lagos et al. (2013) is an effort towards this direction, and the dependence of β on V_c predicted by that model is shown in Fig. 15 of that paper. But since the model in Lagos et al. (2013) only considers ejecting gas out of galaxies, but does not predict what fraction of this escapes from the halo, the model is incomplete. We therefore only use very general and rough features of the dependence of β on V_c and z predicted by Lagos et al. (2013) to motivate our EvoFb model, which assumes a redshift-dependent β .

Lagos et al. (2013) suggest that the mass loading, β , is weaker in starbursts than for quiescent star formation in galaxy disks, because starbursts have higher gas density and molecular gas fraction. While this feature is not included in our model, as it may be too complex for a phenomenological SN feedback model, it has the potential to enhance the reionization redshift and the stellar metallicities of galaxies, so it might be worth investigating it in future work.

4.2 What kind of galaxies reionized the Universe?

Fig. 6 shows some simple statistics of the galaxies producing the ionizing photons. The first row shows the statistics of the stellar mass, M_* , of the galaxies producing ionizing photons, the second row shows the statistics of the dust-extincted rest-frame far-UV absolute magnitude, $M_{\text{AB}}(1500\text{\AA})$, of these galaxies, while the third row shows the statistics of the halo masses, M_{halo} , and the fourth row shows the statistics of the galaxy circular velocity, V_c . For each quantity, the dots in each panel indicate the medians of the corresponding quantity, and the error bars indicate the 5–95% range, with the medians and percentiles determined not by the number of galaxies but by their contributions to the ionizing emissivity at that redshift. The median means that galaxies below it contribute 50% of the ionizing photons at a given redshift, while the 5–95% range indicates that the galaxies within it contribute 90% of the ionizing photons at a given redshift. Each column corresponds to a different SN feedback model. The vertical dashed lines in each panel indicate $z_{\text{re,full}}$, the redshift at which the Universe is fully ionized, for that model, with the numerical values of $z_{\text{re,full}}$ given in the panels in the first row.

From Fig. 6 it is clear that the median of M_* at $z \sim z_{\text{re,full}}$ for each SN feedback model is around $10^8 - 10^9 M_\odot$, the median of $M_{\text{AB}}(1500\text{\AA})$ is around $-17 - -19$, and the median of V_c is around $100 - 200 \text{ km s}^{-1}$. These values indicate that the corresponding galaxies are progenitors of large massive galaxies at $z = 0$. This means in these models, the progenitors of large galaxies make significant contributions to the cosmic reionization. It is also true that the progenitors of large galaxies have already made contributions to the ionizing photons when the Universe was half ionized, i.e. by $z = z_{\text{re,half}}$. This means that a preferential suppression of the SN feedback in very small galaxies is not very effective in boosting $z_{\text{re,half}}$, and to predict a high enough $z_{\text{re,half}}$ by these means usually requires heavy suppression of the SN feedback in very small galaxies, which spoils the

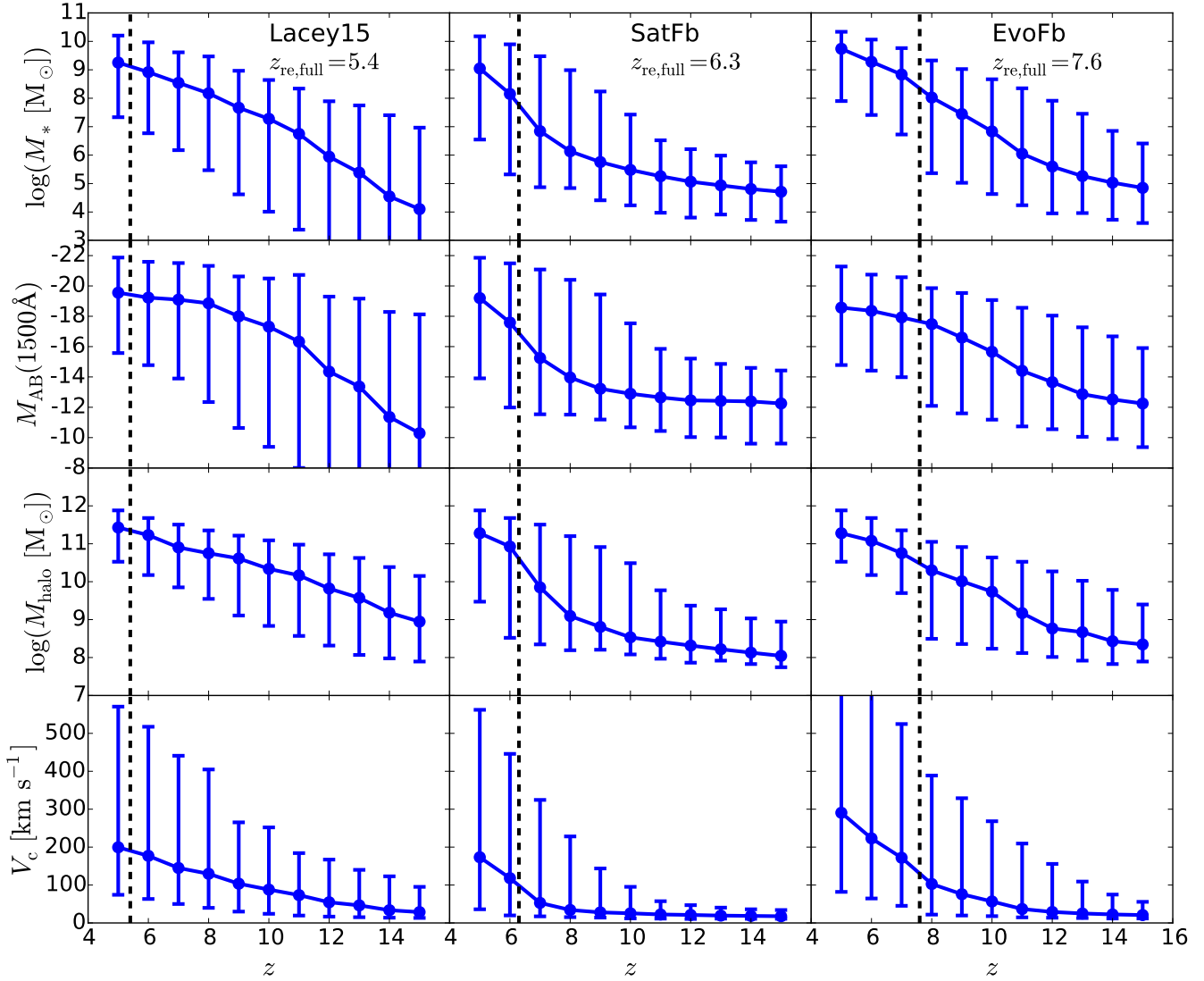


Figure 6. Simple statistics of the galaxies producing ionizing photons. Each column corresponds to a different SN feedback model, with the corresponding model name given in the top of each panel in the first row, along with the value of $z_{\text{re,full}}$, the redshift at which the Universe is fully ionized. The vertical dashed lines in each panel also indicate $z_{\text{re,full}}$. The first row shows the statistics of the stellar mass, M_* , of the galaxies producing ionizing photons, the second row shows the statistics of the dust-extincted rest frame UV magnitude, $M_{\text{AB}}(1500\text{\AA})$, of these galaxies, while the third row shows the statistics of the halo masses, M_{halo} and the fourth row shows the statistics of the galaxy circular velocity, V_c . For each quantity shown in these rows, the dots indicate the medians of the corresponding quantity, and the errorbars the 5 – 95% range, with both the medians and the 5 – 95% ranges being determined by their contributions to the ionizing photon emissivity at that redshift.

agreement with observations of faint galaxies at $z = 0$. This is the reason for the failure of the SatFb model to satisfy all the observational constraints considered in this work.

Fig. 6 also shows that the median of M_{halo} in each SN feedback model is roughly in the range $10^{10} - 10^{11} M_{\odot}$ at $z \sim z_{\text{re,full}}$, which means there are significant contributions to the ionizing photons from large atomic hydrogen cooling halos. This is consistent with the results from Boylan-Kolchin et al. (2014), who show that it is difficult to obtain reionization at $z \sim 8$ mainly from star formation in small atomic cooling halos with $M_{\text{halo}} \sim 10^8 M_{\odot}$.

We also calculated the rest-frame far-UV luminosity functions at $z = 7, 8, 9, 10$ for our 3 different SN feedback models. These predictions are shown in Fig. 7, and com-

pared with recent observational data. The best fit (EvoFb) model is seen to agree quite well with the observations over the whole range $z = 7 - 10$. On the other hand, the other 2 models, which generally have stronger SN feedback at high redshift than the EvoFb model, predict too few low UV luminosity galaxies at $z = 7 - 10$. Note that the current observational limit is $M_{\text{AB}}(1500\text{\AA}) \sim -17 - -18$ at these redshifts, which is close to the median of $M_{\text{AB}}(1500\text{\AA})$ at reionization for the EvoFb model shown in Fig. 6 (for this model, at $z = 8$, the median is $M_{\text{AB}}(1500\text{\AA}) = -17.5$, and the 5 – 95% range is $M_{\text{AB}}(1500\text{\AA}) = -12.1$ to $M_{\text{AB}}(1500\text{\AA}) = -19.8$). Thus the best fit model suggests that the currently observed high redshift galaxy population should contribute about half of the ionizing photons that reionized the Universe.

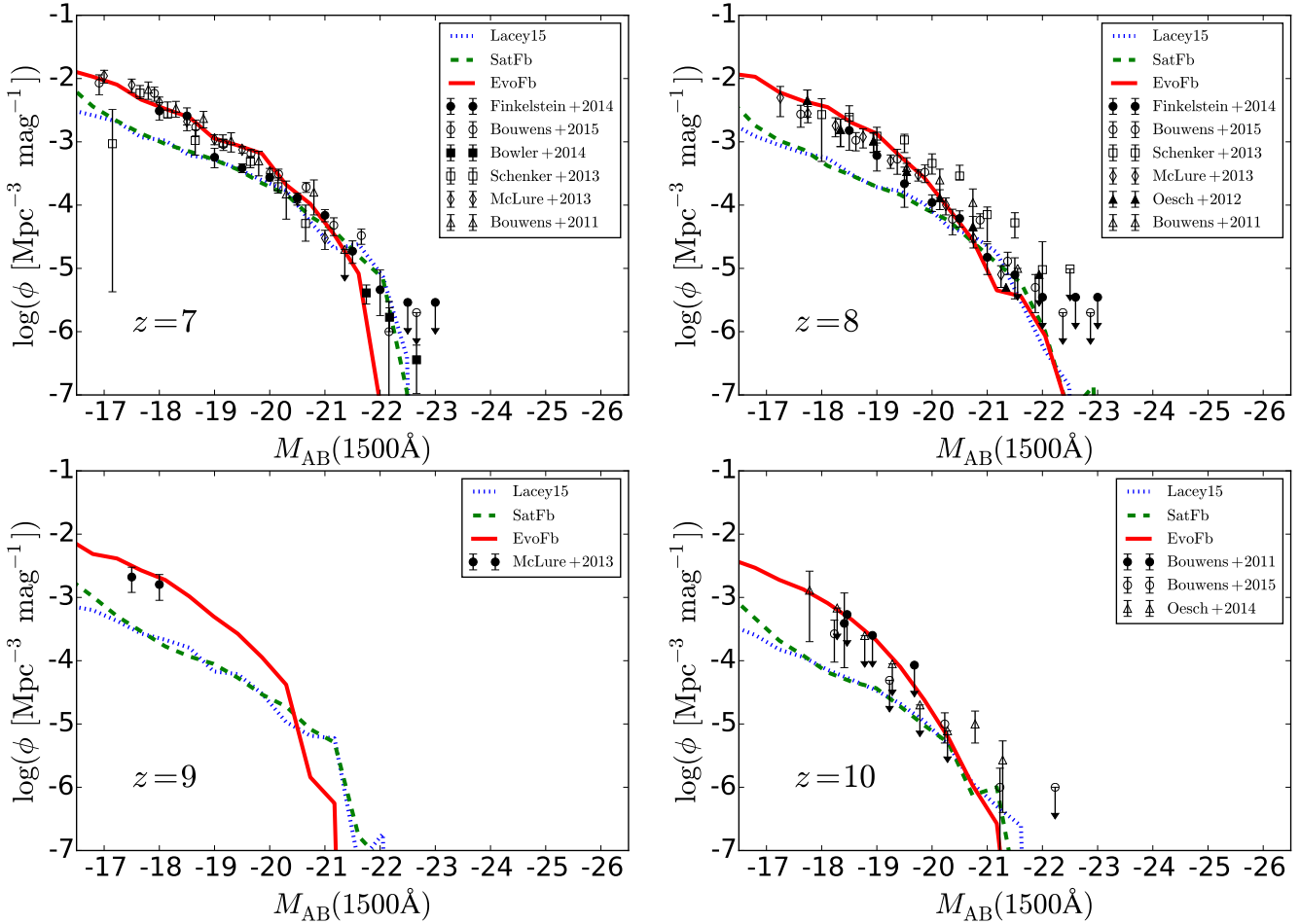


Figure 7. The rest frame far-UV luminosity functions at $z = 7, 8, 9, 10$ for the 3 different SN feedback models. In each panel, the blue dotted line shows the prediction for the Lacey15 model, the dashed green line that for the SatFb model, and the red solid line that for the EvoFb model, while symbols with errorbars indicate observational measurements (Bouwens et al. 2011b,a; Oesch et al. 2012; Schenker et al. 2013; McLure et al. 2013; Finkelstein et al. 2014; Bowler et al. 2014; Oesch et al. 2014; Bouwens et al. 2015).

Fig. 8 shows the fraction of the ionizing photons that are contributed by starbursts at a given redshift (as compared to stars formed quiescently in galaxy disks). Different panels are for different SN feedback models, and the vertical dashed lines indicate $z_{\text{re,full}}$ for the corresponding models. It is clear that at $z \sim z_{\text{re,full}}$, the starburst fractions are high, with $f_{\text{burst}} \approx 0.5$ for the SatFb model and $f_{\text{burst}} \approx 0.8$ for the Lacey15 and EvoFb models. This indicates that starbursts are a major source of the ionizing photons for cosmic reionization.

4.3 The descendants of the galaxies that ionized Universe

For the best fit model, i.e. the EvoFb model, we also identified the $z = 0$ descendants of the galaxies which ionized the Universe. To do this, we ran a simulation with fixed dark matter halo mass resolution $M_{\text{res}} = 7.1 \times 10^7 M_{\odot}$ from $z = 20$ to $z = 0$. This M_{res} is low enough to ensure that we resolve all the atomic cooling halos up to $z = 11$. According to Fig. 3, most of the ionizing photons that reionized the Universe are produced near $z_{\text{re,full}}$, and for the EvoFb

model, $z_{\text{re,full}} = 7.6$. Thus, resolving all the atomic cooling halos up to $z = 11$ ensures that all galaxies which are major sources of the ionizing photons and their star formation histories are well resolved.

In Fig. 9 we show the mass distributions of the $z = 0$ descendants of the objects which produced the photons which reionized the Universe, weighted by the number of ionizing photons produced. The top panel shows the stellar mass of the descendant galaxy, while the bottom panel shows the mass of the descendant dark matter halo. To calculate these, we effectively identify each ionizing photon emitted at $z \geq z_{\text{re,full}}$, then identify the $z = 0$ descendant (galaxy or halo) of the galaxy which emitted it, then construct the probability distribution of descendant mass, giving equal weight to each ionizing photon. The upper panel of Fig. 9 shows that over 50% of the ionizing photons are from the progenitors of large galaxies with $M_* > 3 \times 10^{10} M_{\odot}$, or equivalently, the major ionizing sources have $z = 0$ large galaxies as their descendants. The lower panel of Fig. 9 shows that 50% of the ionizing photons are from the progenitors of high mass dark matter halos at $z = 0$ with $M_{\text{halo}} > 3.7 \times 10^{13} M_{\odot}$, which means that the reionization is

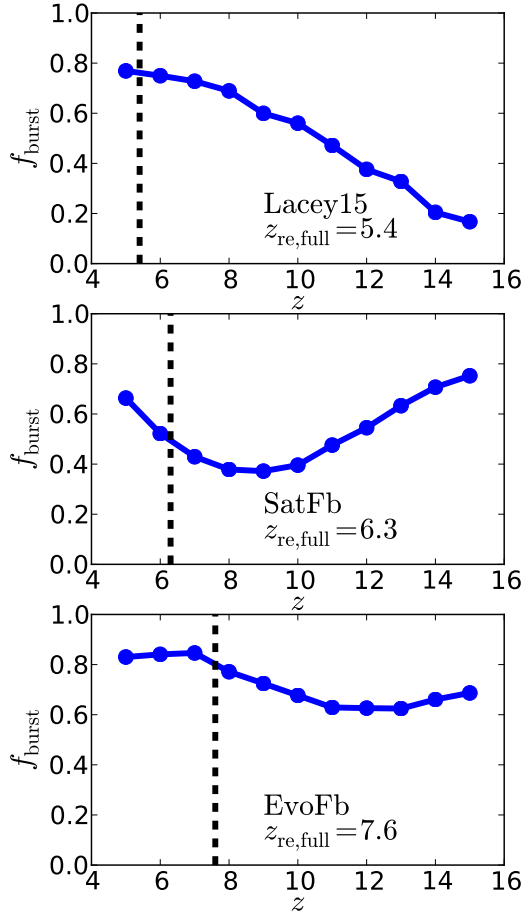


Figure 8. The fraction of the ionizing photon emissivity contributed by starbursts at a given redshift. Different panels are for different SN feedback models, as labelled, and the vertical dashed lines indicate $z_{\text{re,full}}$.

driven mainly by sources at very rare density peaks. These results are consistent with the indications given by Fig. 6.

In Fig. 10, we show the fraction of stellar mass in galaxies at $z = 0$ that was formed before reionization, i.e. at $z \geq z_{\text{re,full}}$, for the best fit model (the EvoFb model). The upper panel shows this for all galaxies, while the lower panel shows this quantity only for galaxies in Milky Way-like halos, defined as halos with $z = 0$ halo mass in the range $5 \times 10^{11} M_{\odot} \leq M_{\text{halo}} \leq 2 \times 10^{12} M_{\odot}$. The upper panel shows that even though the progenitors of the $z = 0$ large galaxies provided about half of the ionizing photons, only a tiny fraction of their stars are formed before reionization, and while the $z = 0$ dwarf galaxies ($M_*(z = 0) < 10^6 M_{\odot}$) contributed only a small fraction of the photons for reionization, their stellar populations typically are dominated by the stars formed before reionization. This is consistent with the hierarchical structure formation picture, because smaller objects formed earlier, and also formation of galaxies in small halos is suppressed after reionization by photoionization feedback. Also note that the ratio of the mass of the stars formed at $z \geq z_{\text{re,full}}$ to the $z = 0$ stellar mass shows considerable scatter for galaxies with $M_*(z = 0) < 10^7 M_{\odot}$, which means the star formation histories of these small galaxies are very diverse.

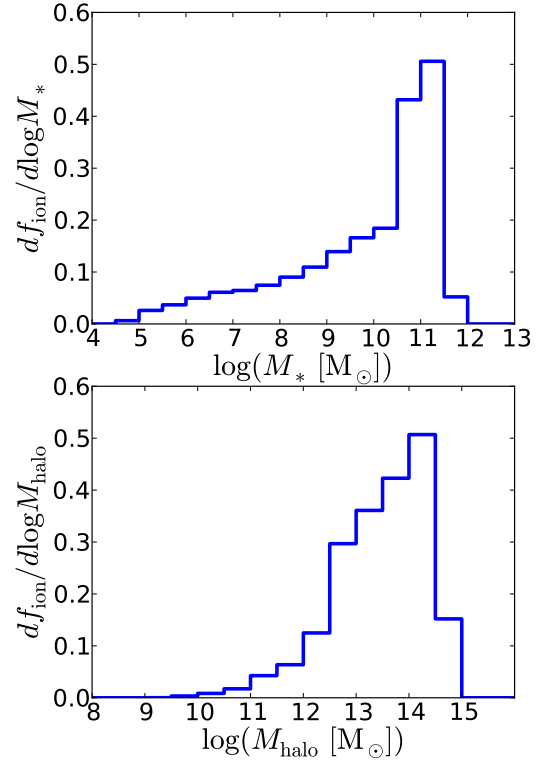


Figure 9. Probability distributions of masses of $z = 0$ descendants of objects which emit ionizing photons at $z \geq z_{\text{re,full}}$, weighted by number of ionizing photons produced. **Upper panel:** Probability distribution of stellar mass of descendant at $z = 0$. **Lower panel:** Probability distribution of halo mass of descendant at $z = 0$.

The lower panel of Fig. 10 shows galaxies in Milky Way-like halos only, but the predicted fraction of stars formed before reionization is in fact very similar to the average over all halos shown in the upper panel. For reference, the short vertical solid black lines indicate the observed stellar masses of several Milky Way satellites (from McConnachie 2012), namely LMC, SMC, Fornax, Sculptor, Leo I, Leo II, Ursa Minor (UrMin) and Hercules. As shown by this panel, the best fit model implies that for the large satellites like the LMC, SMC and Fornax, only tiny fractions of their stellar mass, typically 5% or less, were formed before reionization. However, this fraction increases dramatically with decreasing satellite mass, as does the scatter around the median. For the lowest mass satellites, with stellar mass $M_* < 10^6 M_{\odot}$, including objects like Leo II, Ursa Minor and Hercules, the median fraction increases to around 80%, meaning that most of the satellites in this mass range form the bulk of their stars before reionization, with the 5–95% range in this fraction extending from 40% to 100%, indicating diverse star formation histories for different satellites of the same mass. Satellites in the intermediate mass range $10^6 M_{\odot} \leq M_* < 10^7 M_{\odot}$, like Leo I and Sculptor, have somewhat lower median fractions formed before reionization, around 20–50%, but with an even larger scatter around this median, with the 5–95% range extending nearly from 0% to 100%.

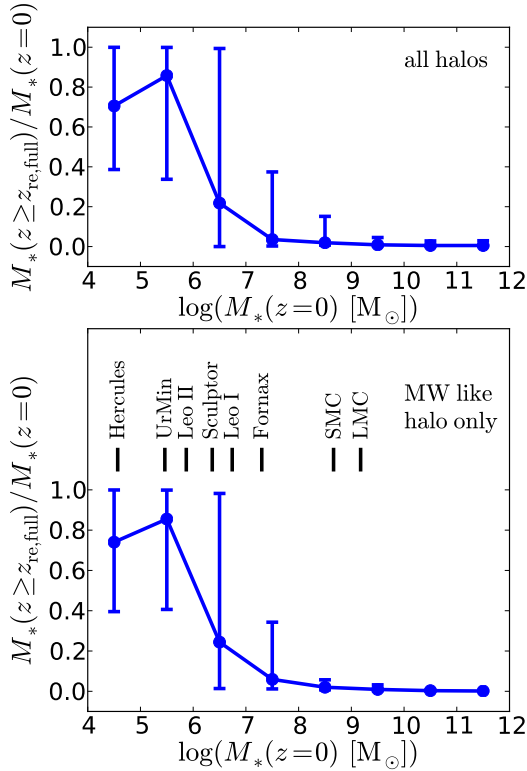


Figure 10. Fraction of stellar mass in galaxies at $z = 0$ which was formed before reionization (i.e. at $z \geq z_{\text{re,full}}$). In both panels, each filled circle shows the median of the ratio in the corresponding $z = 0$ stellar mass bin, while the corresponding error bar indicates the 5 – 95% range of this ratio. **Upper panel:** All galaxies. **Lower panel:** Galaxies in Milky Way-like halos only (defined as halos with $z = 0$ halo mass in the range $5 \times 10^{11} M_{\odot} \leq M_{\text{halo}} \leq 2 \times 10^{12} M_{\odot}$). The short vertical solid black lines indicate the observed stellar masses of several Milky Way satellites, namely LMC, SMC, Fornax, Sculptor, Leo I, Leo II, Ursa Minor (UrMin) and Hercules, for reference (from McConnachie 2012).

5 SUMMARY

We have investigated what constraints can be placed on supernova (SN) feedback by combining a physical model of galaxy formation with critical observations which constrain the strength of feedback in opposite directions. The observational constraints are: the optical and near-IR field luminosity functions (LFs) at $z = 0$; the redshift $z_{\text{re, half}}$, at which the Universe was half reionized; the Milky Way (MW) satellite LF; and the stellar metallicity vs. stellar mass ($Z_* - M_*$) relation for MW satellites. We use the GALFORM semi-analytical model of galaxy formation embedded in the Λ CDM model of structure formation, with 3 different formulations for the mass-loading factor, β , of galactic outflows driven by SN feedback: (a) in the Fiducial model, β is a simple power law in galaxy circular velocity, V_c ; (b) in the Saturated feedback model, β is a broken power law in V_c , with a flat slope at low V_c ; (c) in the Evolving feedback model, β decreases at high redshift, as well as having a break to a shallower slope at low V_c . The Fiducial model was previously tuned by Lacey et al. (2015) to fit a wide range of observational constraints, but

not including reionization or the MW satellites. Our main conclusions are:

(i) The single power law formulation of β as used in the Fiducial model can reproduce the faint ends of the $z = 0$ field LFs and MW satellite LF, but leads to too low $z_{\text{re, half}}$ and too low MW satellite metallicities. This indicates that in this model, the SN feedback is too strong in small galaxies and/or at $z > 8$.

(ii) Simply reducing the SN feedback in small galaxies, as in the Saturated model, does not provide an improvement relative to the single power law formulation of β .

(iii) The Evolving SN feedback model, with weaker SN feedback at high redshifts and stronger SN feedback at low redshifts, seems to be preferred by the above mentioned observational constraints. Including the effects of local reionization may further improve the predictions for the MW satellite LF.

(iv) The physical reasons for the redshift evolution in our phenomenological Evolving SN feedback model could be that a single function of galaxy V_c only captures the effects of the gravitational potential well on the SN feedback, but the SN feedback is likely also to depend on factors such as the cold gas density and metallicity and the molecular gas fraction, which evolve with redshift. However, a more detailed ISM model is required to test the conclusions from this work further.

(v) In all of the SN feedback models analysed in this work, around 50% of the photons which reionize the IGM are emitted by galaxies with stellar masses $M_* \gtrsim 10^9 M_{\odot}$, rest-frame far-UV absolute magnitudes, $M_{\text{AB}}(1500\text{\AA}) \lesssim -18$, galaxy circular velocities $V_c \gtrsim 100 \text{ km s}^{-1}$ and halo masses $M_{\text{halo}} \gtrsim 10^{11} M_{\odot}$ at the redshift $z \sim z_{\text{re, full}}$ at which the Universe is fully reionized. In addition, most of the ionizing photons are predicted to be emitted by galaxies undergoing starbursts, rather than forming stars quiescently. This implies that the currently observed high redshift galaxy population should contribute about half of the ionizing photons that reionized Universe.

(vi) For our best fit model, namely the Evolving feedback model, the $z = 0$ descendants of the major ionizing photon sources are relatively large galaxies with $M_* \gtrsim 10^{10} M_{\odot}$, and are mainly in dark matter halos with $M_{\text{halo}} \gtrsim 10^{13} M_{\odot}$. However, for these galaxies, the fraction of stars formed before reionization is low, while this fraction is high for dwarf galaxies with $z = 0$ stellar masses $M_* < 10^6 M_{\odot}$, even though the progenitors of such dwarfs contribute little to reionizing the Universe. This fraction also shows considerable scatter for the dwarfs, indicating that the star formation histories of these dwarf galaxies are very diverse.

(vii) For satellite galaxies in Milky Way-like halos, our best fit model implies that the fraction of stars formed before reionization is very low for large satellites like the LMC, SMC and Fornax, but reaches very high values for very small satellites with stellar masses $M_* < 10^6 M_{\odot}$, like Leo II, Ursa Minor and Hercules, with median fractions around 80%, indicating that typically these small satellites formed most of their stars before reionization.

ACKNOWLEDGEMENTS

We thank Tom Theuns and Mahavir Sharma for helpful discussions. This work was supported by the Science and Technology Facilities Council grant ST/L00075X/1, and by European Research Council grant GA 267291 (Cosmiway), and SB is supported by STFC through grant ST/K501979/1. This work used the DiRAC Data Centric system at Durham University, operated by the Institute for Computational Cosmology on behalf of the STFC DiRAC HPC Facility (www.dirac.ac.uk). This equipment was funded by BIS National E-infrastructure capital grant ST/K00042X/1, STFC capital grant ST/H008519/1, and STFC DiRAC Operations grant ST/K003267/1 and Durham University. DiRAC is part of the National E-Infrastructure.

REFERENCES

Asplund M., Grevesse N., Sauval A. J., Scott P., 2009, *ARA&A*, 47, 481
 Bate M. R., 2012, *MNRAS*, 419, 3115
 Baugh C. M., Lacey C. G., Frenk C. S., Granato G. L., Silva L., Bressan A., Benson A. J., Cole S., 2005, *MNRAS*, 356, 1191
 Benson A. J., Bower R. G., Frenk C. S., Lacey C. G., Baugh C. M., Cole S., 2003, *ApJ*, 599, 38
 Benson A. J., Lacey C. G., Baugh C. M., Cole S., Frenk C. S., 2002, *MNRAS*, 333, 156
 Bouwens R. J. et al., 2011a, *Nature*, 469, 504
 Bouwens R. J. et al., 2011b, *ApJ*, 737, 90
 Bouwens R. J. et al., 2015, *ApJ*, 803, 34
 Bower R. G., Benson A. J., Malbon R., Helly J. C., Frenk C. S., Baugh C. M., Cole S., Lacey C. G., 2006, *MNRAS*, 370, 645
 Bowler R. A. A. et al., 2014, *MNRAS*, 440, 2810
 Boylan-Kolchin M., Bullock J. S., Garrison-Kimmel S., 2014, *MNRAS*, 443, L44
 Cole S., Lacey C. G., Baugh C. M., Frenk C. S., 2000, *MNRAS*, 319, 168
 Couchman H. M. P., Rees M. J., 1986, *MNRAS*, 221, 53
 Davé R., Katz N., Oppenheimer B. D., Kollmeier J. A., Weinberg D. H., 2013, *MNRAS*, 434, 2645
 de Boer T. J. L. et al., 2012, *A&A*, 544, A73
 Dekel A., Silk J., 1986, *ApJ*, 303, 39
 Driver S. P. et al., 2012, *MNRAS*, 427, 3244
 Efstathiou G., 1992, *MNRAS*, 256, 43P
 Finkelstein S. L. et al., 2014, *ArXiv e-prints*
 Font A. S. et al., 2011, *MNRAS*, 417, 1260
 Hopkins P. F., Quataert E., Murray N., 2012, *MNRAS*, 421, 3488
 Klypin A., Kravtsov A. V., Valenzuela O., Prada F., 1999, *ApJ*, 522, 82
 Komatsu E. et al., 2011, *ApJS*, 192, 18
 Kuposov S. et al., 2008, *ApJ*, 686, 279
 Lacey C. G. et al., 2015, *ArXiv e-prints arXiv:1509.08473*
 Lagos C. d. P., Lacey C. G., Baugh C. M., 2013, *MNRAS*, 436, 1787
 Larson R. B., 1974, *MNRAS*, 169, 229
 Lewis A., 2008, *Phys. Rev. D*, 78, 023002
 McConnachie A. W., 2012, *AJ*, 144, 4
 McLure R. J. et al., 2013, *MNRAS*, 432, 2696

Moore B., Ghigna S., Governato F., Lake G., Quinn T., Stadel J., Tozzi P., 1999, *ApJ*, 524, L19
 Norberg P. et al., 2002, *MNRAS*, 336, 907
 Oesch P. A. et al., 2012, *ApJ*, 759, 135
 Oesch P. A. et al., 2014, *ApJ*, 786, 108
 Okamoto T., Gao L., Theuns T., 2008, *MNRAS*, 390, 920
 Parkinson H., Cole S., Helly J., 2008, *MNRAS*, 383, 557
 Planck Collaboration et al., 2014, *A&A*, 571, A16
 Planck Collaboration et al., 2015, *ArXiv e-prints*
 Raičević M., Theuns T., Lacey C., 2011, *MNRAS*, 410, 775
 Schaye J. et al., 2015, *MNRAS*, 446, 521
 Schenker M. A. et al., 2013, *ApJ*, 768, 196
 Thoul A. A., Weinberg D. H., 1996, *ApJ*, 465, 608
 Vargas L. C., Geha M., Kirby E. N., Simon J. D., 2013, *ApJ*, 767, 134
 Vogelsberger M. et al., 2014, *Nature*, 509, 177
 White S. D. M., Frenk C. S., 1991, *ApJ*, 379, 52